ICASE

ON THE RELATION BETWEEN THE UPWIND-DIFFERENCING SCHEMES OF GODUNOV, ENGQUIST-OSHER AND ROE

Bram van Leer

Report No. 81-11

March 16, 1981

INSTITUTE FOR COMPUTER APPLICATIONS IN SCIENCE AND ENGINEERING
NASA Langley Research Center, Hampton, Virginia

Operated by the

UNIVERSITIES SPACE USRA RESEARCH ASSOCIATION

ON THE RELATION BETWEEN THE UPWIND-DIFFERENCING SCHEMES OF GODUNOV, ENGQUIST-OSHER AND ROE

Bram van Leer
Institute for Computer Applications in Science and Engineering
and
Leiden State University, Leiden, The Netherlands

ABSTRACT

The upwind-differencing first-order schemes of Godunov, Engquist-Osher and Roe are discussed on the basis of the inviscid Burgers equations. The differences between the schemes are interpreted as differences between the approximate Riemann solutions on which their numerical flux-functions are based. Special attention is given to the proper formulation of these schemes when a source term is present. Second-order two-step schemes, based on the numerical flux-functions of the first-order schemes are also described. The schemes are compared in a numerical experiment, and recommendations on their use are included.

This work was supported under NASA Contract No. NAS1-14472 while the author was in residence at ICASE, NASA Langley Research Center, Hampton, VA 23665.

1. Introduction

Upwind differencing, while trivial for a diagonalized hyperbolic system, is difficult to achieve when the difference scheme has to be written in conservation form. The oldest and most complicated version is due to Godunov [1] [2]; the increasing popularity of upwind differencing recently has lead to a variety of simpler implementation techniques. A review of these is given by Harten, Lax and Van Leer [3].

Among the recent additions to the family of upwind conservative schemes the method of Engquist and Osher [4] [5] is closest to the original Godunov scheme, while the method of Roe [6] [7] offers the greatest simplification In the present paper the differences between these schemes are discussed on the basis of the inviscid Burgers equation. The first-order accurate schemes are explained in Sections 2, 3, and 4 for the homogeneous equation; Section 6 describes how to include a source term and Section 7 how to achieve second-order accuracy in a two-step format. Their rendition of a stationary shock and a transonic expansion is discussed in Section 5 and illustrated in the numerical experiments of Section 8. Section 9 rounds off with recommendations regarding the application of these schemes to single conservation laws and systems of conservation laws.

2. Godunov's method

Godunov's [1] [2] method for integrating a hyperbolic system of conservation laws

$$u_t + [f(u)]_x = 0, \tag{1}$$

is a scheme in conservation form:

$$(u_i^{n+1} - u_i^n)/\Delta t + \{F(u_i^n, u_{i+1}^n) - F(u_{i-1}^n, u_i^n)\}/\Delta x = 0; \tag{2}$$

here u_i^n represents the average value at time $t^n = n\Delta t$ in the computational zone centered on $x_i = i\Delta x$. The numerical flux-function $F_G(u_i^n, u_{i+1}^n)$ in the Godunov scheme is taken to be the flux value arising at $x_{i+\frac{1}{2}}$ in the exact solution of the initial-value problem with a piecewise uniform initial distribution

$$u^n(x) = u_i^n \qquad x_i - \Delta x/2 < x < x_i + \Delta x/2. \tag{3.1}$$

That is, if

$$u(x,t) = v(x/t; u_L, u_R)\ , \tag{3.2}$$

is the (weak) similarity solution of the Riemann problem with initial values

$$u = \begin{cases} u_L & x < 0 \\ u_R & x > 0, \end{cases} \tag{3.3}$$

then

$$F_G(u_i^n, u_{i+1}^n) = f[v(0; u_i^n, u_{i+1}^n)]\ . \tag{4}$$

For Burgers' equation in the inviscid limit,

$$u_t + (\tfrac{1}{2}u^2)_x = 0, \tag{5}$$

the similarity solution to the initial-value problem (3.2) is

$$u_L \le u_R \text{ (expansion)} \quad \begin{cases} v = u_L & x/t \le u_L \\ v = x/t & u_L < x/t < u_R \\ v = u_R & x/t \ge u_R \end{cases} \tag{6.1}$$

$$u_L > u_R \text{ (shock)} \quad \begin{cases} v = u_L & x/t < u_S = \tfrac{1}{2}(u_L + u_R) \\ v = u_R & x/t > u_S \end{cases} \tag{6.2}$$

For numerical reasons it is useful to distinguish in the formula for $F_G(u_L,u_R)$ three cases:

(i) fully supersonic/subsonic

$$F_G(u_L,u_R) = \begin{cases} \frac{1}{2}u_L^2 & u_L,u_R > 0 \\ \frac{1}{2}u_R^2 & u_L,u_R < 0 \end{cases} , \tag{7.1}$$

(ii) transonic expansion

$$F_G(u_L,u_R) = 0 \qquad u_L \leq 0 \leq u_R , \tag{7.2}$$

(iii) transonic shock

$$F_G(u_L,u_R) = \begin{cases} \frac{1}{2}u_L^2 & u_L > u_S \geq 0 \geq u_R \\ \frac{1}{2}u_R^2 & u_L \geq 0 > u_S > u_R \end{cases} . \tag{7.3}$$

These cases are illustrated in Figures 1, 2 and 3. The references to a sonic speed (= 0) arises from the use of (5) in transonic aerodynamics.

In order to combine the formulas (7) in one compact algorithm, we follow Engquist and Osher by introducing

$$u^+ \equiv \max(u,0) , \tag{8.1}$$

$$u^- \equiv \min(u,0) , \tag{8.2}$$

$$u = u^+ + u^- , \tag{8.3}$$

$$|u| = u^+ - u^- ; \tag{8.4}$$

we then have

$$F_G(u_L,u_R) = \max\left[\tfrac{1}{2}(u_L^+)^2 , \tfrac{1}{2}(u_R^-)^2\right] . \tag{9}$$

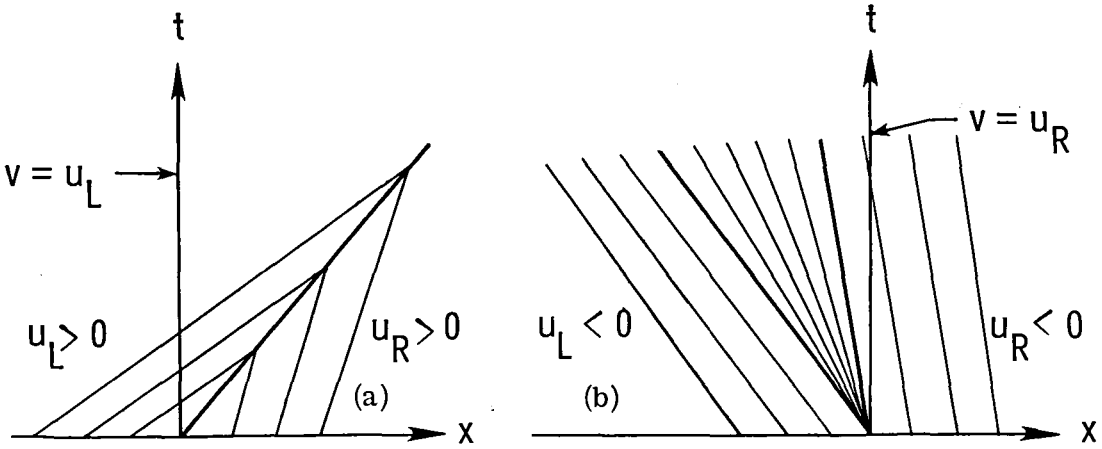

Figure 1. Riemann solution: (x,t) diagrams for case (i), with $u_L > u_R > 0$ (a); $u_L < u_R < 0$ (b).

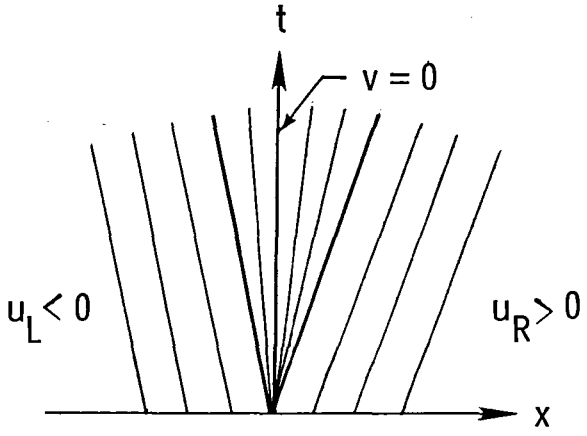

Figure 2. (x,t) diagram for case (ii).

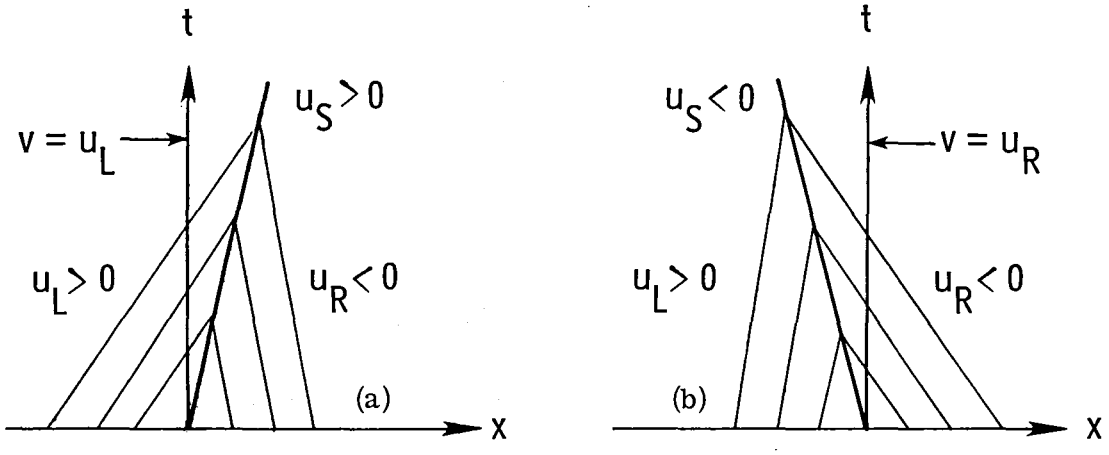

Figure 3. (x,t) diagram for case (iii), with $u_S > 0$ (a); $u_S < 0$ (b).

3. The Engquist-Osher scheme

The Engquist-Osher [4] [5] scheme for integrating (1) also has the conservation form (2) and tacitly assumes the initial-value distribution to be (3.1); its numerical flux-function is

$$F_{EO}(u_L,u_R) = f(u_L) + \int_{u_L}^{u_R} A^-(u)du$$

$$= f(u_R) - \int_{u_L}^{u_R} A^+(u)du \qquad (10)$$

$$= \tfrac{1}{2}[f(u_L)+f(u_R)] - \tfrac{1}{2}\int_{u_L}^{u_R}|A(u)|du,$$

where the matrices $A^+(u)$, $A^-(u)$ and $|A(u)|$ are related to

$$A(u) \equiv df/du \qquad (11)$$

by an extension of (8). For precise definitions and a description of the integration path used for the integrals in (10), see [5] or the review [3].

For Burgers' equation (5) the above recipe boils down to

$$F_{EO}(u_L,u_R) = \tfrac{1}{2}u_L^2 + \int_{u_L}^{u_R} u^-du$$

$$= \tfrac{1}{2}u_R^2 - \int_{u_L}^{u_R} u^+du \qquad (12)$$

$$= \tfrac{1}{2}(\tfrac{1}{2}u_L^2+\tfrac{1}{2}u_R^2) - \tfrac{1}{2}\int_{u_L}^{u_R}|u|du\ .$$

The integrals over u in (12) are defined in phase space, without reference to any mapping onto the (x,t) plane. We may, however, introduce a mapping in the style of (3.2), namely,

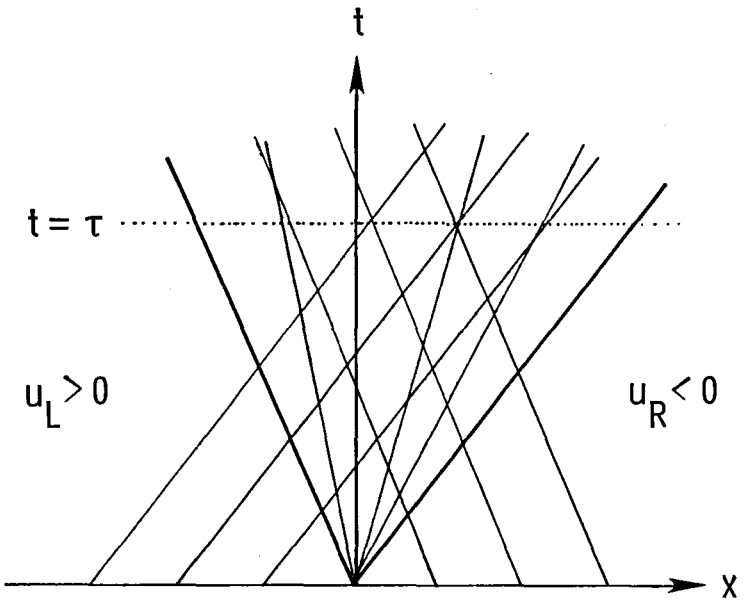

Figure 4. Approximate Riemann solution in the Engquist-Osher scheme: (x,t) diagram for case (iii). The multi-valued solution at $t = \tau$ is displayed in Figure 5.

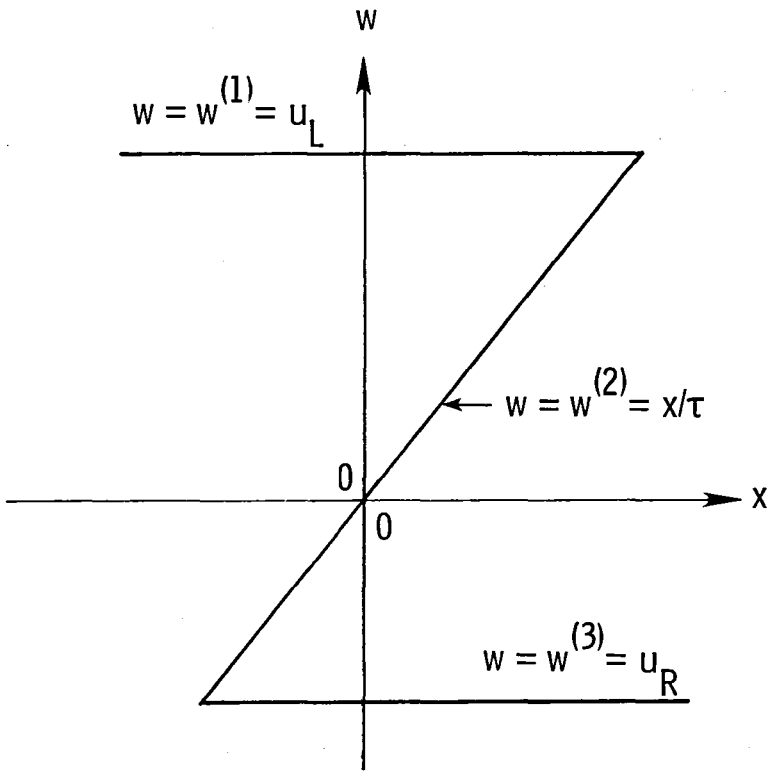

Figure 5. Approximate Riemann solution at $t = \tau$.

(13) $u(x,t) = w(x/t;u_L,u_R) \qquad \min(u_L,u_R) \le u \le \max(u_L,u_R).$

and consider $w(x/t;u_L,u_R)$ an approximation to the exact solution $v(x/t;u_L,u_R)$ of the Riemann problem (3.3). It follows that w is the following function of x/t:

$$
\begin{aligned}
&w = u_L && x/t \le u_L \ , \\
&w = x/t && \min(u_L,u_R) < x/t < \max(u_L,u_R) \ , \\
&w = u_R && x/t \ge u_R \ .
\end{aligned}
\tag{14}
$$

In relating $F_{E0}(u_L,u_R)$ to $w(0;u_L,u_R)$ after the example of (4), caution is required, since, for $u_L > u_R$, w becomes multi-valued in the domain $u_L \ge x/t \ge u_R$. Specifically, we have three branches

$$
w^{(1)} = u_L, \ w^{(2)} = x/t, \ w^{(3)} = u_R \qquad\qquad u_L \ge x/t \ge u_R. \tag{15}
$$

The picture associated with this case is that of an overturned centered compression wave or folded characteristic field (see Figures 4 and 5); in the exact Riemann solution (6) such a wave would be replaced by a shock discontinuity.

The proper formula for $F_{E0}(u_L,u_R)$ in terms of $w(x/t;u_L,u_R)$, equivalent to (12), is

$$
F_{E0}(u_L,u_R) = \sum_k (-1)^{k-1} w^{(k)}(0;u_L,u_R), \tag{16}
$$

where the sum is taken over all branches present at $x/t = 0$.

In the cases distinguished earlier, (12) or (16) yields

$$\text{(i)}\quad F_{E0}(u_L,u_R) = F_G(u_L,u_R) = \begin{cases} \tfrac{1}{2}u_L^2 & u_L,u_R > 0 \\ \tfrac{1}{2}u_R^2 & u_L,u_R < 0 \end{cases},$$

$$\text{(17)}\quad \text{(ii)}\quad F_{E0}(u_L,u_R) = F_G(u_L,u_R) = 0 \ ,$$

$$\text{(iii)}\quad F_{E0}(u_L,u_R) = \tfrac{1}{2}u_L^2 + \tfrac{1}{2}u_R^2 \neq F_G(u_L,u_R) \ .$$

As indicated in [4], these formulas combine into

$$\text{(18)}\qquad F_{E0}(u_L,u_R) = \tfrac{1}{2}(u_L^+)^2 + \tfrac{1}{2}(u_R^-)^2 \ .$$

The difference between the Godunov and Engquist-Osher schemes lies entirely in the treatment of a transonic compression (iii). The latter scheme is the simpler one, since it does away with one test, namely, a test for the sign of u_S or for the maximum of $\tfrac{1}{2}(u_L^+)^2$ and $\tfrac{1}{2}(u_R^-)^2$.

4. Roe's method

Roe's [6] [7] method for integrating (1) again has the conservation form (2) and employs the initial-value distribution (3.1). Its numerical flux-function is defined as

$$\text{(19)}\qquad F_R(u_i^n,u_{i+1}^n) = f[w(0;u_i^n,u_{i+1}^n)],$$

where $w(x/t;u_L,u_R)$ is the exact solution of the Riemann problem (3.3) for the locally linearized system

$$\text{(20.1)}\qquad w_t + A(u_L,u_R)w_x = 0.$$

The approximate Jacobian $A(u_L,u_R)$ is constructed such as to satisfy the discrete version of (11)

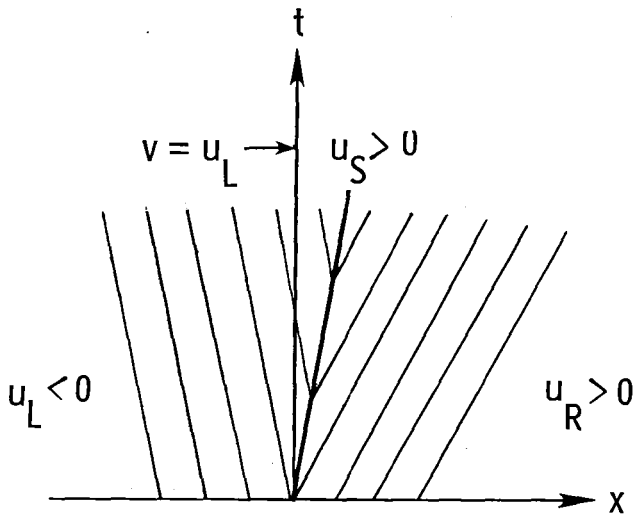

Figure 6. Approximate Riemann solution in Roe's scheme: (x,t) diagram for case (iii), with $u_S > 0$, showing the expansion shock.

$$f(u_R) - f(u_L) = A(u_L,u_R)(u_R - u_L). \tag{20.2}$$

For a scalar equation like (5), eq. (20.2) uniquely determines $A(u_L,u_R)$:

$$A(u_L,u_R) = \tfrac{1}{2}(u_L + u_R) = u_S; \tag{21}$$

thus, the Riemann problem for the linear equation (20.1) with (21) has the similarity solution

$$w(x/t,u_L,u_R) = \begin{cases} u_L & x/t < u_S \\ u_R & x/t > u_S \end{cases}. \tag{22}$$

In all cases (i), (ii) and (iii) this yields

$$F_R(u_L,u_R) = \begin{cases} \tfrac{1}{2}u_L^2 & u_S > 0 \\ \tfrac{1}{2}u_R^2 & u_S < 0 \end{cases}. \tag{23}$$

The difference with Godunov's method lies in the treatment of an expansion: where the exact Riemann solution, used in Godunov's method, would include an expansion fan, Roe's method puts in a so-called expansion shock (see Figure 6).

The numerical flux-function (23) deviates from the Godunov flux (7) only in case (ii), when the expansion is transonic. The computational simplification is, again, the elimination of one test.

Rewriting (23) as an approximation to the Enquist-Osher flux (12):

$$F_R(u_L,u_R) = \tfrac{1}{2}(\tfrac{1}{2}u_L^2 + \tfrac{1}{2}u_R^2) - \tfrac{1}{2}\left|\tfrac{1}{2}(u_L+u_R)\right| (u_R - u_L), \tag{24}$$

we see that, for Burgers' equation, Roe's scheme is identical to the scheme of Murman and Cole [8], used in transonic aerodynamics. The latter is

known to occasionally yield numerical results that include a (physically inadmissible) expansion shock. This is a direct consequence of the admission of an expansion shock in the underlying approximate Riemann solution.

5. Steady-shock and sonic-point representation

The fluxes in the schemes of Godunov and Engquist-Osher differ only on meshes where the data constitute a transonic compression; therefore, numerical results from these schemes differ only if a transonic shock, in particular, a stationary shock, is present. Likewise, the results of Roe's scheme will differ from those of Godunov's scheme only if a transonic expansion is present.

For Burgers' equation (5), Godunov's scheme admits the following stationary discrete representation of a stationary shock connecting the states $u_L > 0$ and $u_R = -u_L < 0$:

$$
\begin{aligned}
u_i &= u_L \qquad && i \le -1, \\
u_0 &= u_M \qquad && u_L \ge u_M \ge u_R, \\
u_i &= -u_L \qquad && i \ge 1.
\end{aligned}
\tag{25}
$$

This is the only stationary distribution admitted by the scheme.

The interior value u_M indicates the sub-grid position x_S of the shock; by conservation we have, (see Figure 7a):

$$u_L(x_S + \tfrac{1}{2}\Delta x) + u_R(\tfrac{1}{2}\Delta x - x_S) = u_M \Delta x, \tag{26.1}$$

or

$$x_S = \tfrac{1}{2}\Delta x \; u_M/u_L. \tag{26.2}$$

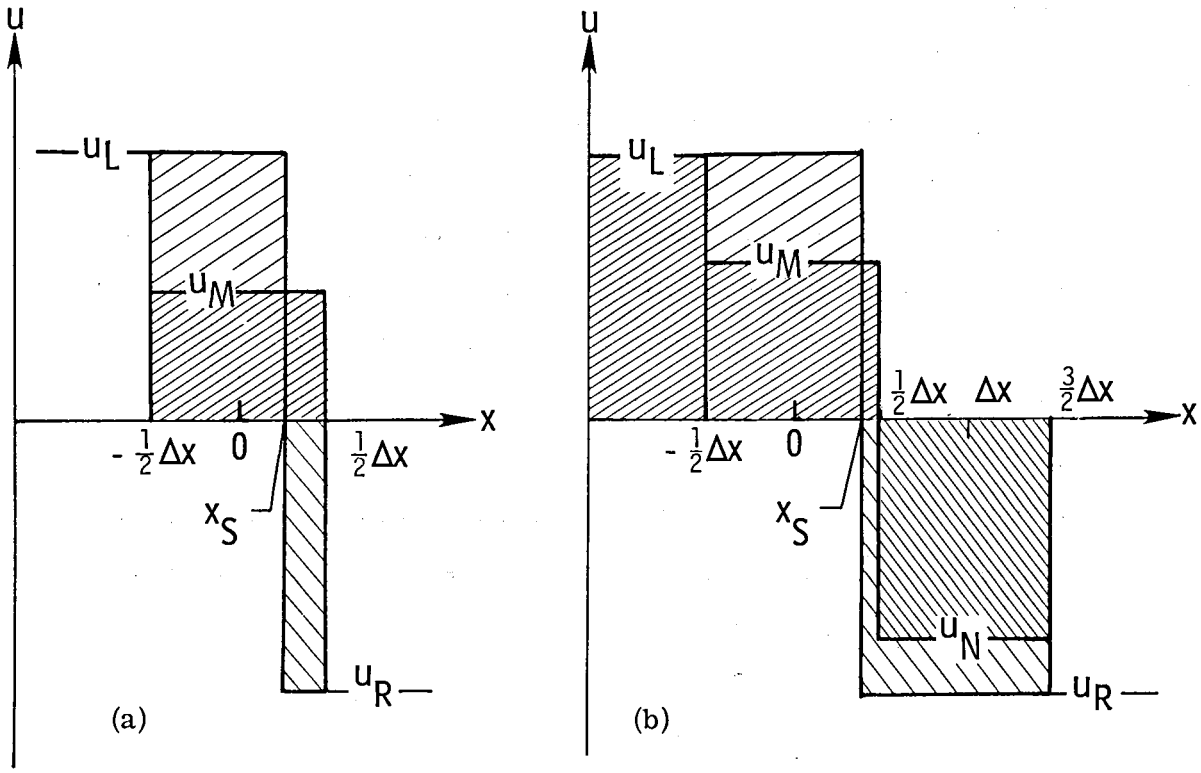

Figure 7. Fitting a shock discontinuity to stationary discrete shocks yielded by the schemes of Godunov or Roe (a) and Engquist-Osher (b). The numerical values u_M and u_N represent the average value of u in the intervals $(-\frac{1}{2}\Delta x, \frac{1}{2}\Delta x)$ and $(\frac{1}{2}\Delta x, \frac{3}{2}\Delta x)$. A sub-grid distribution representing a shock transition from u_L to u_R at x_S must have the same integral as the numerical solution. In case (a) the integrals from $-\frac{1}{2}\Delta x$ to $\frac{1}{2}\Delta x$ are compared, in case (b) from $-\frac{1}{2}\Delta x$ to $\frac{3}{2}\Delta x$.

A shock standing exactly on the boundary of a zone will be represented without any interior value.

The Engquist-Osher scheme admits discrete steady shock-profiles with, in general, two interior states:

$$
\begin{aligned}
u_i &= u_L \qquad && i \leq -1, \\
u_0 &= u_M \qquad && u_L \geq u_M \geq 0, \\
u_i &= u_N \qquad && 0 \geq u_N \geq -u_L, \\
u_i &= -u_L \qquad && i \geq 2,
\end{aligned}
\tag{27.1}
$$

where u_M and u_N are constrained by

$$
\tfrac{1}{2}u_M^2 + \tfrac{1}{2}u_N^2 = \tfrac{1}{2}u_L^2. \tag{27.2}
$$

Again, this is the only stationary distribution admitted by the scheme.

The pair of interior states indicates the sub-grid position of the shock; by conservation we have (see Figure 7b):

$$
u_L(x_S + \tfrac{1}{2}\Delta x) + u_R(\tfrac{3}{2}\Delta x - x_S) = (u_M + u_N)\Delta x, \tag{28.1}
$$

or

$$
x_S = \tfrac{1}{2}\Delta x(u_M + u_N + u_L)/u_L. \tag{28.2}
$$

A shock standing exactly in the middle of a zone will be represented with only one interior value.

The representation of a stationary shock by Roe's scheme is the same as by Godunov's scheme, at least for Burgers' equation. However, Roe's scheme also admits as a stationary solution the expansion shock

$$u_i = u_L < 0 \qquad i \leq -1,$$

(29)

$$u_i = -u_L > 0 \qquad i \geq 0.$$

The tendency of the scheme to produce such a discontinuity spoils the smoothness of the numerical solution near a sonic point. The other schemes do not have this problem. It is easily solved, anyway, by introducing in the approximate Riemann solution (22) some spreading of the expansion shock. For Burgers' equation, Roe's scheme essentially will turn into Godunov's scheme; for a nonlinear hyperbolic system, however, it will still remain a simpler scheme.

A transonic shock profile, steady or not, obtained with any of the upwind schemes, has the property that the interior zones can not influence the exterior solution. Inversely, in a transonic expansion computed with the Roe-Murman-Cole scheme, the zone with the value closest to the sonic value can not be influenced by the rest of the grid (see Figure 8).

6. Inclusion of a source term

When approximating the equation

$$u_t + [f(u)]_x = s(x) \tag{30}$$

with any upwind scheme, it is not sufficient to add the source term to the right-hand side of (2); we must also change the initial-value distribution implied in our numerical model. Instead of assuming that it is piecewise uniform, as in (3.1), we rather take it to be piecewise stationary, that is,

$$[f(u^n(x))]_x = s(x) \qquad x_i - \Delta x/2 < x < x_i + \Delta x/2, \tag{31.1}$$

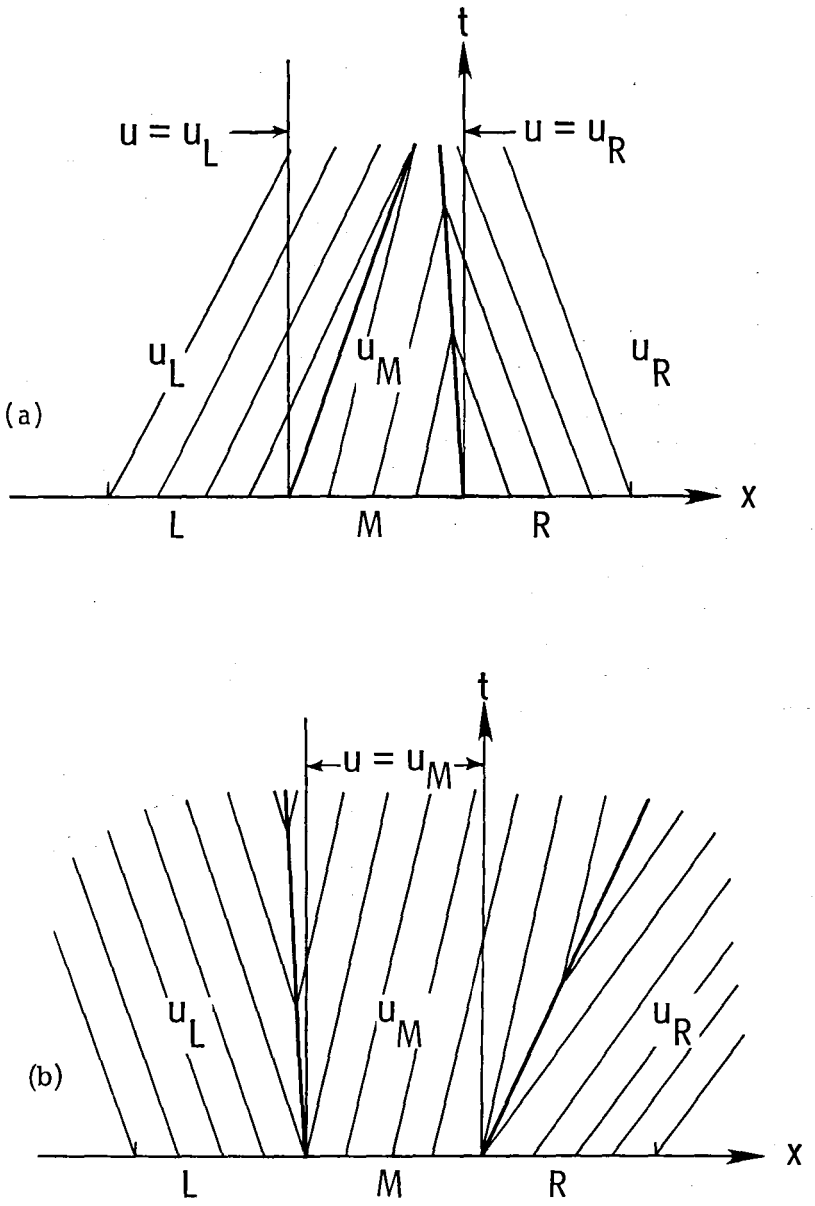

Figure 8. Two (x,t) diagrams showing the influence, through Godunov's scheme, of the adjacent zones on a zone inside a shock (a) and the influence, through Roe's scheme, of an almost sonic zone on the adjacent zones (b). In (a), the fluxes at the boundaries of zone M do not depend on u_M; in (b) they depend only on u_M.

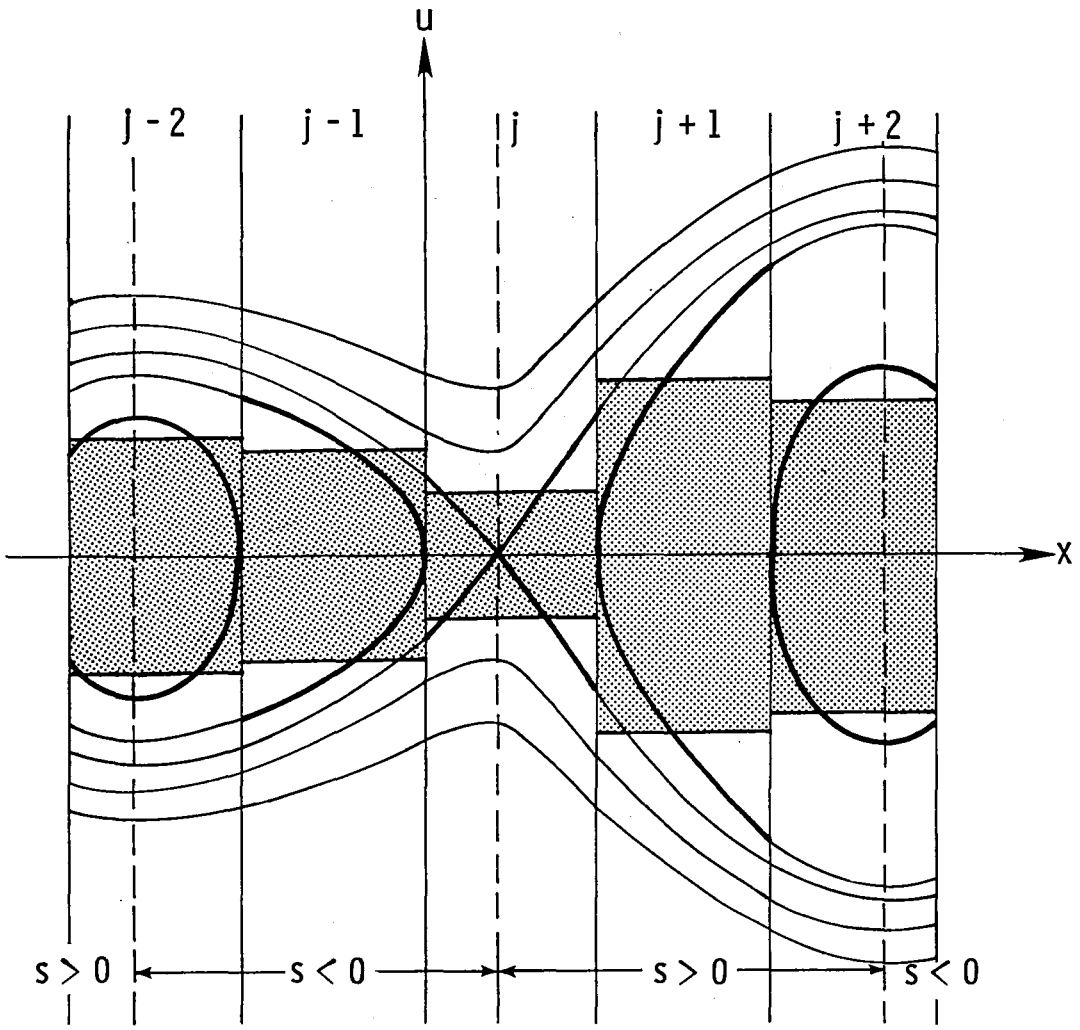

Figure 9. Stationary solutions of eq. (30) for some source term s(x). In each zone the heavy line traces the positive and the negative branch of the smallest continuous steady solution. The average value on these branches is indicated by the upper and lower boundary of the shaded area. If the average value in a zone falls in the range of the shaded area, a continuous stationary solution can not be realized.

with

$$\frac{1}{\Delta x}\int_{x_i - \Delta x/2}^{x_i + \Delta x/2} u^n(x)dx = u_i^n. \tag{31.2}$$

This extension preserves a fundamental property of the homogeneous scheme, namely, that a zone-average can change only through the finite-amplitude waves entering from the zone boundaries. Moreover, if the numerical solution globally tends to a steady state, it will be the zone-averaged exact steady state almost everywhere (that is, provided that the scheme, like the three considered here, can render a shock transition in a finite number of zones).

As before, the initial values on either side of a zone boundary become the arguments of the numerical flux-function. The full scheme reads

$$(u_i^{n+1} - u_i^n)/\Delta t + \left\{F(u^n_{(i+\frac{1}{2})-}, u^n_{(i+\frac{1}{2})+}) - F(u^n_{(i-\frac{1}{2})-}, u^n_{(i-\frac{1}{2})+})\right\}/\Delta x = s_i^n, \tag{32.1}$$

with

$$s_i \equiv \frac{1}{\Delta x}\int_{x_{i-\frac{1}{2}}}^{x_{i+\frac{1}{2}}} s(x)dx. \tag{32.2}$$

For the inhomogeneous Burgers equation

$$u_t + (\tfrac{1}{2}u^2)_x = s(x) \tag{33}$$

the initial-value representation must satisfy

$$\tfrac{1}{2}[u^n(x)]^2 = \tfrac{1}{2}[u^n(x_{(i-\frac{1}{2})+})]^2 + \int_{x_{i-\frac{1}{2}}}^{x} s(x')dx' \qquad x_i - \Delta/2 < x < x_i + \Delta/2 \tag{34}$$

under the constraint (31.2). This constraint, however, is not strong enough to define a unique distribution in each zone, since the distribution may (and, in some zones, must) contain a discontinuity. Uniqueness can be achieved by selecting the distribution with, say, the weakest possible shock.

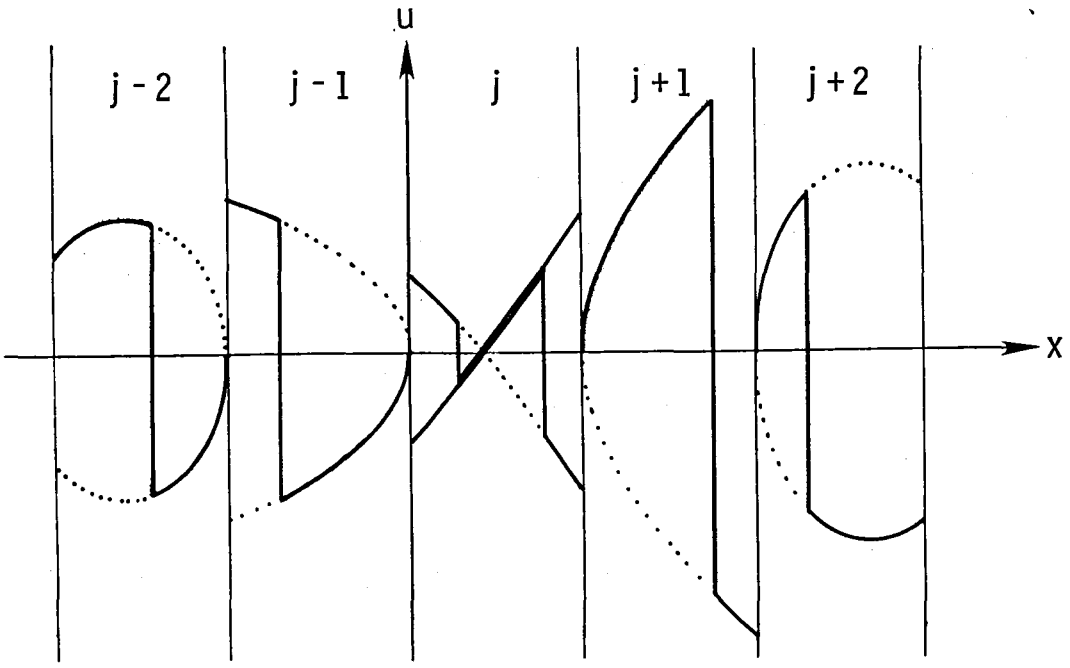

Figure 10. Examples of steady structure with a discontinuity, in the zones shown in Figure 9. A (steady) shock connects the upper and lower branch of the smallest continuous steady solution for the zone considered. In zone j two different possibilities are shown.

If we take Δx small enough to ensure that $s(x)$ does not change sign more than once in any zone, the following algorithm for the piecewise construction of $u^n(x)$ is adequate. First, determine for the zone under consideration the smallest continuous solution (see Figure 9). Let ω_i^n be the average value on the positive branch of this solution; then the stationary distribution inside zone i will be continuous if

$$|u_i^n| \geq \omega_i^n. \tag{35}$$

If this condition is satisfied, we search, iteratively, for the continuous distribution with the proper zone average. If it is violated, the stationary distribution will include parts of the upper and lower branch of the smallest continuous distribution, connected by a shock positioned so as to achieve the proper average value (see Figure 10).

When using the upwind scheme to approach a globally stationary solution of (33), any zone containing a sonic point must be treated with special care, since the chance of numerically realizing the exact transonic structure without a shock is zero. Specifically, in order to prevent the zone-boundary values from flipping sign, making global convergence impossible, smoothing may be introduced (see Figure 11).

In a zone containing a stationary shock, no particular interior structure is needed to ensure global convergence, since the zone cannot influence its neighbors (see earlier Figure 8a). After convergence one may insert the proper structure by enforcing continuity across the zone boundaries (see Figure 12).

In the numerical experiment of Section 8 we approximated the above procedure, in allowing only s_i to enter the zone-boundary values. Specifically, we used

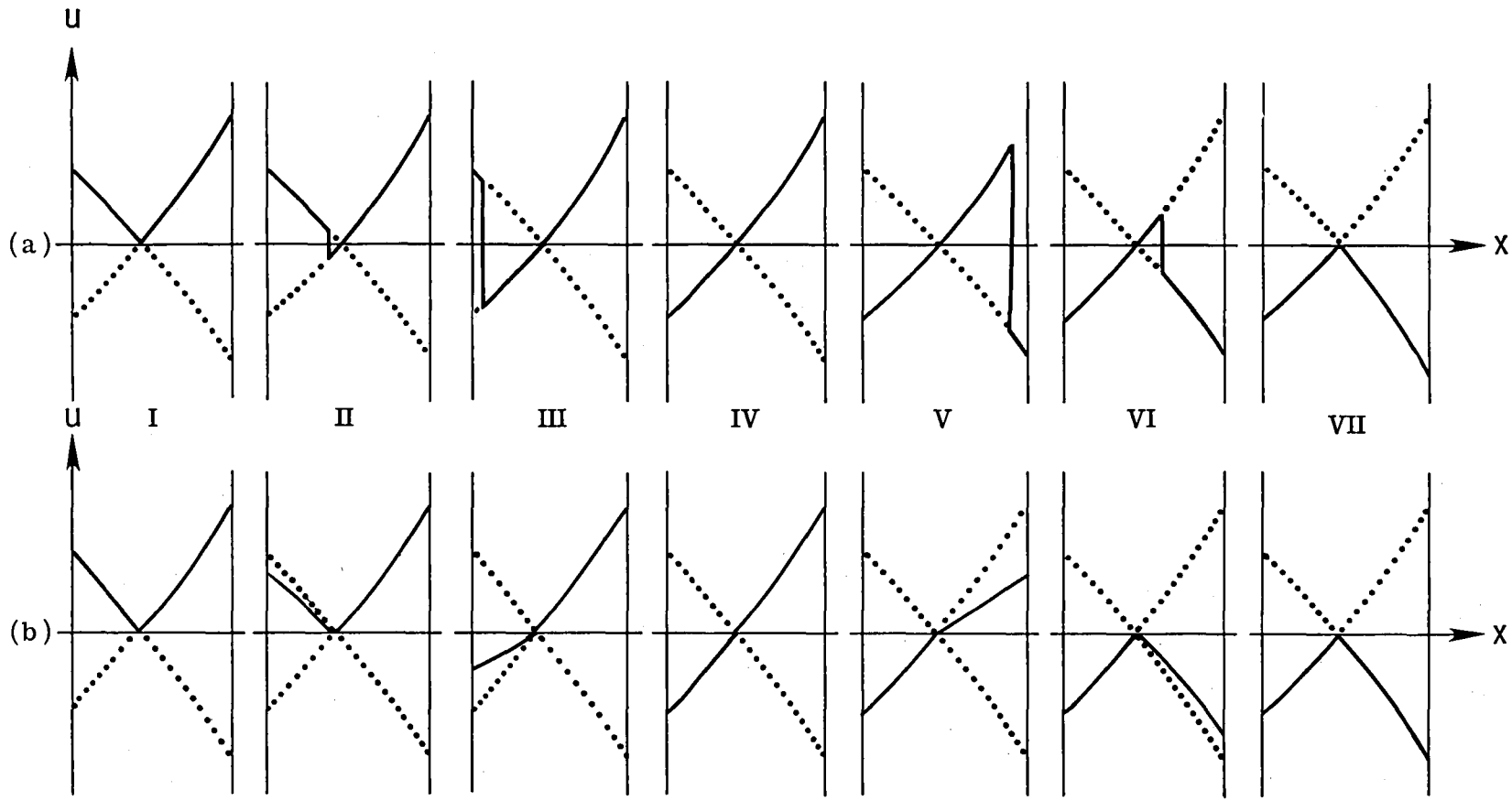

Figure 11. (a) A sequence of stationary structures close to the transonic expansion (graph IV), ordered by decreasing zone-average. Going from III to IV, and from IV to V, the slight change in zone-average causes one boundary value to flip its sign. (b) The solutions have been smoothed on the side where the shock occurs, so that the boundary values now vary continuously with the zone-average. The structures are not stationary but will allow convergence to the smooth transonic solution IV.

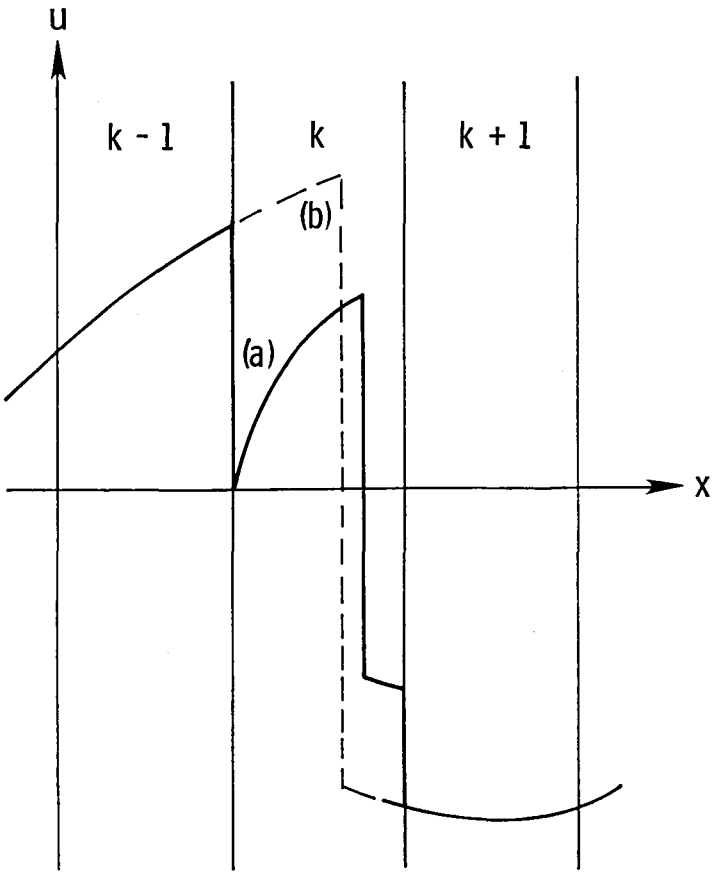

Figure 12. Shock structure in a globally stationary solution. Global convergence of the zone averages to a steady solution containing a shock has been obtained, say, with Godunov's scheme. For zone k containing the shock the scheme had adopted the structure (a), based on the smallest continuous steady solution for that zone. This may now be replaced by the stationary solution (b) that smoothly connects to the solution in zones k-1 and k+1.

$$u^n(x_{(i\pm\frac{1}{2})\mp}) = \mathrm{sgn}(u_i^n)\sqrt{(u_i^n)^2 \pm \min\{|s_i|\Delta x, (u_i^n)^2\}\mathrm{sgn}(s_i)}\ . \tag{36}$$

In a zone that includes a sonic point the error in the boundary values is $0(\Delta x)$; elsewhere in the smooth part of the numerical solution it is $0((\Delta x)^2)$.

The technique of computing the boundary values in a zone from a locally stationary solution can easily be extended to systems of conservation laws of the form

$$u_t + [f(u,x)]_x = s(x). \tag{37}$$

7. Second-order upwind schemes

Any first-order upwind scheme for Eq. (30) can be changed into a second-order method by first advancing the cell-boundary values, to be used in the numerical flux-function, to the intermediate time level $t^{n+\frac{1}{2}} = t^n + \frac{1}{2}\Delta t$. In obtaining these values, the interaction between cells can be fully ignored. This observation, due to Hancock [9], has led to a drastic simplification of second-order upwind schemes since these first were formulated for systems of conservation laws by Van Leer [10].

We assume that the initial values form a piecewise linear distribution:

$$u^n(x) = u_i^n + (x - x_i)\frac{(\delta u)_i^n}{\Delta x} \qquad x_{i-\frac{1}{2}} < x < x_{i+\frac{1}{2}}\ , \tag{38}$$

with

$$(\delta u)_i^n = \mathrm{ave}(u_{i+1}^n - u_i^n,\ u_i^n - u_{i-1}^n); \tag{39}$$

ave(a,b) is an averaging procedure to be specified later. We particularly need the initial boundary values inside cell i

$$u^n_{(i\pm\frac{1}{2})\mp} = u^n_i \pm \tfrac{1}{2}(\delta u)^n_i. \tag{40.1}$$

These boundary values are now advanced to $t^{n+\frac{1}{2}}$ by

$$u^{n+\frac{1}{2}}_{(i\pm\frac{1}{2})\mp} = u^n_{(i\pm\frac{1}{2})\mp} - \frac{\Delta t}{2\Delta x}\left\{f(u^n_{(i+\frac{1}{2})-}) - f(u^n_{(i-\frac{1}{2})+})\right\} + \frac{\Delta t}{2} s_i . \tag{40.2}$$

The full scheme becomes

$$(u^{n+1}_i - u^n_i)/\Delta t + \left\{F\left(u^{n+\frac{1}{2}}_{(i+\frac{1}{2})-}, u^{n+\frac{1}{2}}_{(i+\frac{1}{2})+}\right) - F\left(u^{n+\frac{1}{2}}_{(i-\frac{1}{2})-}, u^{n+\frac{1}{2}}_{(i-\frac{1}{2})+}\right)\right\}/\Delta x = s_i. \tag{41}$$

The function ave(a,b) is chosen such that it tends to $\frac{1}{2}(a+b)$ if a and b are subsequent finite differences of a smooth solution, but tends to the smallest value where the solution is not smooth. Examples can be found in [11],[10]; we chose a refined formula due to Van Albada [12]

$$\text{ave}(a,b) = \frac{(b^2+c^2)a + (a^2+c^2)b}{a^2 + b^2 + 2c^2}, \tag{42.1}$$

where c^2 is a small bias of the order $0((\Delta x)^3)$.

The weighted averaging prevents central differencing across a discontinuity in the solution or in its first derivative which would lead to numerical oscillations. It is an effective way of administering artificial dissipation wherever needed and nowhere else. By rewriting (42.1) as

$$\text{ave}(a,b) = \frac{a+b}{2}\left\{1 - \frac{(a-b)^2}{a^2 + b^2 + 2c^2}\right\}, \tag{42.2}$$

we see that, wherever the solution is smooth, the artificial-viscosity coefficient generally is of the order $0((\Delta x)^2)$. In a smooth extremum the coefficient grows to $0(\Delta x)$; the bias $2c^2$ in the denominator prevents a further increase of the viscosity that could lead to an undesirable clipping phenomenon (see [13, Appendix]).

With regard to Burgers' equation, an acceptable expression for the bias is

$$c^2 = (u_{max} - u_{min})^2 (\Delta x)^3 / (x_{max} - x_{min})^3, \tag{43}$$

where u_{max} and u_{min} are certain upper and lower bounds of the numerical solution, fixed a priori or determined at each time level, and $x_{max} - x_{min}$ is the length-scale of the problem.

8. Numerical comparison

The performance of the three schemes was tested on the basis of the periodic initial-value problem

$$u_t + (\tfrac{1}{2}u^2)_x = (\pi/2)\sin[2\pi(x-\xi)] \qquad 0 \le x \le 1,\ 0 \le \xi << 1 \tag{44.1}$$

$$u(x,0) = 0, \tag{44.2}$$

$$u(0,t) = u(1,t). \tag{44.3}$$

The solution tends to the steady state

$$u(x,\infty) = \begin{cases} +\sin\pi(x-\xi) & 0 \le x < \xi + \tfrac{1}{2} \\ -\sin\pi(x-\xi) & \xi + \tfrac{1}{2} < x \le 1, \end{cases} \tag{45}$$

including a sonic point at $x = \xi$ and a shock at $x = x_s = \xi + \tfrac{1}{2}$. For Δx we chose a value of 1/16; the zones were centered on $x_i = (i - \tfrac{1}{2})\Delta x$, $i = 1,\ldots,16$. For ξ we chose 0, $\tfrac{1}{4}\Delta x$, and $\tfrac{1}{2}\Delta x$, in order to achieve different sub-grid shock positions. The Courant-Friedrichs-Lewy condition on the timestep, based on the maximum characterisitc speed (=1) in the steady solution is

(46) $$\frac{\Delta t}{\Delta x} \leq 1;$$

accordingly we used $\Delta t = \frac{1}{2}\Delta x$ or $\Delta t = \Delta x$.

Table 1 shows the number of steps N_ε it took the schemes to converge according to the L_1- criterion

(4.7) $$\sum_{i=1}^{16} |u_i^n - u_i^{n-1}| < \varepsilon,$$

with $\varepsilon = 1 \times 10^{-3}$ or 1×10^{-6}, and $\Delta t = \frac{1}{2}\Delta x$ or (for Godunov's scheme only) $\Delta t = \Delta x$. When the time-step is doubled, N_ε appears to be halved. The L_1-error E_ε was evaluated with respect to the zone-averaged exact solution, for the smallest value of ε. The sub-grid shock positions in Table 1 were calculated with aid of eqs. (26.1) and (28.1), approximately valid because the source term is small in the shock region.

The converged solutions for $\varepsilon = 1 \times 10^{-6}$ are listed in Table 2; these are independent of Δt. The zone-averaged exact solution is given for comparison. For $\xi = \frac{1}{4}\Delta x$ and $\frac{1}{2}\Delta x$ the error in the zone with the sonic point is comparable to the value in the zone, as anticipated with the use of Eq. (36).

The results of Roe's scheme happen to be identical to those of Godunov's scheme; in particular, no expansion shock shows up. The reason is that, with the use of the boundary values (36), a sonic point in a zone is always moved to a boundary; in this case Roe's flux function (23) yields the same value (=0) as Godunov's (7.2). Furthermore, the initial average value in the zone ultimately containing the sonic point was close to the steady value to begin with.

The results of the Engquist-Osher scheme are identical to the Godunov-Roe results except for the expected spread in the shock profile for $\xi = 0$

$\xi/\Delta x$	N_ε				E_ε		$(x_S - \frac{1}{2})/\Delta x$	
	$\varepsilon = 1 \times 10^{-3}$		$\varepsilon = 1 \times 10^{-6}$		$\varepsilon = 1 \times 10^{-6}$		$\varepsilon = 1 \times 10^{-6}$	
	G, R	EO	G, R	EO	G, R	EO	G, R	EO
0	62	61	112 [55]	111	8.8×10^{-3}	4.6×10^{-2}	0	0
$\frac{1}{4}$	68	66	138 [70]	136	9.6×10^{-3}	1.8×10^{-2}	.23	.26
$\frac{1}{2}$	52	52	88 [42]	88	4.6×10^{-3}	4.6×10^{-3}	$\frac{1}{2}$	$\frac{1}{2}$

Table 1. Number of steps N_ε till convergence, L_1-error E_ε, and steady-shock position x_S, for the initial-value problem (44), solved with the first order schemes of Godunov (G), Engquist-Osher (EO) and Roe (R). Mesh: $\Delta x = 1/16$, $\Delta t = \frac{1}{2}\Delta x$ or Δx (G only, numbers between brackets).

i	$u_i^{N_\varepsilon}$, u_i^{∞}							
	$\xi/\Delta x = 0$			$\xi/\Delta x = \frac{1}{4}$			$\xi/\Delta x = \frac{1}{2}$	
	G, R	EO	exact	G, R	EO	exact	G, R, EO	exact
1	.13795	.13795	.09786	.09778	.09778	.04899	0.00000	0.00000
2	.30373	.30373	.28982	.25516	.25516	.24259	.19321	.19478
3	.47702	.47702	.47064	.43185	.43184	.42687	.37899	.38207
4	.63587	.63587	.63337	.59602	.59602	.59474	.55021	.55468
5	.77180	.77180	.77177	.73869	.73869	.73976	.70028	.70597
6	.87889	.87889	.88051	.85367	.85367	.85635	.82344	.83013
7	.95276	.95276	.95540	.93631	.93631	.94003	.91496	.92240
8	.99044	.69352	.99359	.98329	.88033	.98759	.97132	.97921
9	-.99044	-.69352	-.99359	-.52996	-.42699	-.49739	.00000	-.00000
10	-.95276	-.95276	-.95540	-.96441	-.96441	-.96847	-.97132	-.97921
11	-.87889	-.87889	-.88051	-.89927	-.89927	-.90254	-.91496	-.92240
12	-.77180	-.77180	-.77177	-.79997	-.79997	-.80192	-.82344	-.83013
13	-.63587	-.63587	-.63337	-.67047	-.67047	-.67048	-.70028	-.70597
14	-.47702	-.47702	-.47064	-.51616	-.51616	-.51328	-.55021	-.55468
15	-.30373	-.30373	-.28982	-.34426	-.34426	-.33635	-.37899	-.38207
16	-.13795	-.13795	-.09786	-.16827	-.16827	-.14649	-.19321	-.19478

Table 2. Converged numerical solutions and zone-averaged asymptotic solutions for the experiments of Table 1 with $\varepsilon = 1 \times 10^{-6}$, $\Delta t = \frac{1}{2}\Delta x$.

and $\frac{1}{4}\Delta x$. The sub-grid shock positions are slightly, but no significantly, more accurate than for the other schemes. Likewise, convergence with Engquist-Osher scheme is faster, but not significantly so.

Better results (Tables 3 and 4) were obtained with the second-order versions of the schemes. Convergence was achieved in 10 - 35% fewer steps than with the first-order schemes, and the local error near the sonic point is now of the same order as elsewhere outside the shock.

The Engquist-Osher scheme still yields a shock structure with two interior zones. For the second-order Godunov scheme we checked that the use of algebraic averaging of differences

$$\text{ave}(a,b) = \tfrac{1}{2}(a+b), \tag{48}$$

causes the numerical shock to overshooot and undershoot.

The results of Roe's scheme are practically, but not exactly, identical to the Godunov results, indicating a slightly different transient behavior. Again, the internal structure (36) in the zones, in combination with the particular choice of initial values, provides a safeguard against the occurrence of an expansion shock.

In order to make the problem more challenging, we changed the initial values (44.2), for $\xi = 0$, into

$$u_i^0 = \begin{cases} 1 & i = 1,\ldots,8 \\ -1 & i = 9,\ldots,16, \end{cases} \tag{49}$$

including an expansion shock at $x = 0$. The results are listed in Tables 5 and 6. Among the first-order schemes Roe's scheme now requires 30% more steps than the other schemes: apparently, the expansion shock is not so easily dissipated by Roe's scheme. Among the second-order schemes the discrepancy gets worse: the results of Roe's scheme quickly converge to the wrong solution, including the full initial expansion shock.

$\xi/\Delta x$	N_ε			E_ε			$(x_S - \frac{1}{2})/\Delta x$		
	G2,R2	G2a	EO2	G2, R2	G2a	EO2	G2, R2	G2a	EO2
0	75	76	75	1.4×10^{-3}	3.1×10^{-2}	2.9×10^{-2}	0	0	0
$\frac{1}{4}$	89	92	89	1.3×10^{-3}	2.2×10^{-3}	4.7×10^{-3}	.24	.19	.26
$\frac{1}{2}$	79	79	79	1.3×10^{-3}	1.7×10^{-3}	1.3×10^{-3}	$\frac{1}{2}$	$\frac{1}{2}$	$\frac{1}{2}$

Table 3. The quantities N_ε, E_ε and x_S ($\varepsilon = 1 \times 10^{-6}$) for the initial-value problem (44), solved with the second-order two-step schemes based on the numerical flux-functions of Godunov (G2, G2a), Engquist-Osher (EO2) and Roe (R2). In G2a the algebraic average (48) is used instead of (42.1). Mesh: $\Delta x = 1/16$, $t = \frac{1}{2}\Delta x$.

i	$u_i^{N_\varepsilon}$, u_i^{∞}				
	$\xi/\Delta x = 0$				
	G2	G2a	R	E0	exact
1	.09814	.09814	.09815	.09814	.09786
2	.28976	.28967	.28976	.28975	.28982
3	.47012	.46981	.47012	.47012	.47064
4	.63242	.63201	.63242	.63239	.63337
5	.77076	.76909	.77076	.77086	.77177
6	.87879	.88201	.87880	.87839	.88051
7	.95647	.92357	.95648	.95804	.95540
8	.98761	1.20652	.98761	.76751	.99359
9	-.98761	-1.20652	-.98761	-.76751	-.99359
10	-.95647	-.92357	-.95648	-.95804	-.95540
11	-.87879	-.88201	-.87880	-.87839	-.88051
12	-.77076	-.76909	-.77076	-.77086	-.77177
13	-.63242	-.63201	-.63242	-.63239	-.63337
14	-.47012	-.46981	-.47012	-.47012	-.47064
15	-.28976	-.28967	-.28976	-.28975	-.28982
16	-.09814	-.09814	-.09815	-.09814	-.09786

Table 4. Converged numerical solutions and zone-averaged asymptotic solutions for the experiments of Table 3, with $\varepsilon = 1 \times 10^{-6}$, $\Delta t = \frac{1}{2}\Delta x$.

i	$u_i^{N_\varepsilon}$, u_i^{∞}							
	$\xi/\Delta x = \frac{1}{4}$					$\xi/\Delta x = \frac{1}{2}$		
	G2	G2a	R	EO	Exact	G2, R2, EO	G2a	exact
1	.04916	.04917	.04916	.04916	.04899	0.00000	0.00000	0.00000
2	.24249	.24244	.24249	.24248	.24259	.19468	.19465	.19478
3	.42635	.42610	.42635	.42639	.42687	.38160	.38141	.38207
4	.59379	.59344	.59379	.59364	.59474	.55379	.55348	.55468
5	.73871	.73726	.73871	.73933	.73976	.70492	.70373	.70597
6	.85462	.85711	.85462	.85231	.85635	.82844	.83000	.83013
7	.94080	.91445	.94080	.95106	.94003	.92282	.90418	.92240
8	.98172	1.15231	.98172	.95622	.98759	.97371	1.08877	.97921
9	-.49587	-.60164	-.49587	-.47889	-.49739	.00000	.00000	-.00000
10	-.96449	-1.01358	-.96449	-.96440	-.96847	-.97371	-1.08877	-.97921
11	-.90232	-.89318	-.90232	-.90235	-.90254	-.92282	-.90418	-.92240
12	-.80042	-.80067	-.80042	-.80041	-.80192	-.82844	-.83000	-.83013
13	-.66948	-.66861	-.66948	-.66948	-.67048	-.70492	-.70373	-.70597
14	-.51252	-.51223	-.51252	-.51252	-.51328	-.55379	-.55348	-.55468
15	-.33603	-.33589	-.33603	-.33603	-.33635	-.38160	-.38141	-.38207
16	-.14650	-.14649	-.14650	-.14650	-.14649	-.19468	-.19465	-.19478

Table 4 (continuation)

$\xi/\Delta x$	N_ε						E_ε	
	G	R	EO	G2	R2	EO2	R	R2
0	170	30	169	77	99	76	5.7×10^{-1}	1.4×10^{-3}

Table 5. The quantities N_ε and E_ε ($\varepsilon = 1 \times 10^{-6}$) for the initial-value problem (44.1), (49), (44.3), solved with both first- and second-order upwind schemes. Scheme R converges to the wrong weak solution. Mesh: $\Delta x = 1/16$, $\Delta t = \frac{1}{2}\Delta x$.

i	$u_i^{N_\varepsilon}$, u_i^∞		
	R	R2	exact
1	1.00000	.09815	.09786
2	1.03596	.28976	.28982
3	1.09933	.47012	.47064
4	1.17699	.63242	.63337
5	1.25564	.77076	.77177
6	1.32417	.87880	.88051
7	1.37431	.95648	.95540
8	1.40069	.98762	.99359
9	-1.40069	-.98762	-.99359
10	-1.37431	-.95648	-.95540
11	-1.32417	-.87880	-.88051
12	-1.25564	-.77076	-.77177
13	-1.17699	-.63242	-.63337
14	-1.09933	-.47012	-.47064
15	-1.03596	-.28976	-.28982
16	-1.00000	-.09815	-.09786

Table 6. Converged numerical solutions and zone-averaged asymptotic solution for the experiments of Table 5 with schemes R and R2. Note the expansion shock in the results of R. Parameters: $\xi = 0$, $\varepsilon = 1 \times 10^{-6}$, $\Delta t = \frac{1}{2}\Delta x$.

Finally, Tables 7 and 8 show the same quantitites as Tables 1 and 2 for experiements in which, in the first-order schemes, the source-term dependence of zone-boundary values was dropped. It took the schemes of Engquist-Osher and Godunov 15 - 25% more steps than previously to converge to a much less accurate solution. Roe's scheme is now unstable: it yields an expansion shock where a smooth transonic transition should be; the amplitude of this shock grows linearly with time. The reason is that, across the zone that should contain the sonic point (say, zone j), we always have (see earlier Figure 8b)

$$F_R(u_{j-1}^n, u_j^n) = F_R(u_j^n, u_{j+1}^n) = \tfrac{1}{2}(u_j^n)^2, \tag{50}$$

so that the scheme reduces to

$$u_j^n = u_j^0 + n\Delta t s_j. \tag{51}$$

8. Recommendations

For a scalar conservation law like Burgers' equation there seems to be little reason to abandon Godunov's first-order scheme in favor of the first-order Engquist-Osher scheme. The slight simplification in the flux calculation is accompanied by a degradation of steady-shock representation and no significant acceleration of the convergence to a steady state. The simplification achieved in Roe's first-order scheme is too drastic: the scheme can not be used "as is" near a sonic point.

Both Godunov and Engquist-Osher schemes become appreciably more elaborate when applied to a nonlinear hyperbolic system like the one-dimensional Euler equations. The interpretation of the Engquist-Osher scheme as a Godunov-type scheme in which any shock in the solution of a local Riemann problem is replaced by an overturned centered compression wave, remains valid. This modification

$\xi/\Delta x$	N_ε			E_ε			$(x_S - \frac{1}{2})/\Delta x$		
	Gu	Ru	EOu	Gu	Ru	EOu	Gu	Ru	EOu
0	135	-	135	6.0×10^{-2}	unstable	9.5×10^{-2}	0	-	0
$\frac{1}{4}$	174	-	172	6.1×10^{-2}	unstable	6.7×10^{-2}	.22	-	.24
$\frac{1}{2}$	103	103	103	4.7×10^{-2}	4.7×10^{-2}	4.7×10^{-2}	$\frac{1}{2}$	$\frac{1}{2}$	$\frac{1}{2}$

Table 7. The quantities N_ε, E_ε and x_S ($\varepsilon = 1 \times 10^{-6}$) for the initial-value problem (44), solved with the first-order upwind schemes under the assumption of piecewise uniform initial values (3.1). (The label "u" in Gu, Ru, EOu stands for "uniform".)
Mesh: $\Delta x = 1/16$, $\Delta t = \frac{1}{2}\Delta x$.

i	$u_i^{N_\varepsilon}$, u_i^{∞}							
	$\xi/\Delta x = 0$			$\xi/\Delta x = \frac{1}{4}$			$\xi/\Delta x = \frac{1}{2}$	
	Gu	EOu	exact	Gu	EOu	exact	Gu, Ru, EOu	exact
1	.19509	.19509	.09786	.13828	.13828	.04899	0.00000	0.00000
2	.38268	.38268	.28982	.33330	.33330	.24259	.27324	.19478
3	.55557	.55557	.47064	.51176	.51175	.42687	.46109	.38207
4	.70711	.70711	.63337	.66976	.66976	.59474	.62678	.55468
5	.83147	.83147	.77177	.80171	.80171	.73976	.76677	.70597
6	.92388	.92388	.88051	.90266	.90266	.85635	.87646	.83013
7	.98078	.98078	.95540	.96879	.96879	.94003	.95191	.92240
8	1.00000	.70711	.99359	.99759	.89488	.98759	.99035	.97921
9	-1.00000	-.70711	-.99359	-.54359	-.44088	-.49739	.00000	-.00000
10	-.98078	-.98078	-.95540	-.98796	-.98796	-.96847	-.99035	-.97921
11	-.92388	-.92388	-.88051	-.94026	-.94026	-.90254	-.95191	-.92240
12	-.83147	-.83147	-.77177	-.85632	-.85632	-.80192	-.87646	-.83013
13	-.70711	-.70711	-.63337	-.73932	-.73932	-.67048	-.76677	-.70597
14	-.55557	-.55557	-.47064	-.59368	-.59368	-.51328	-.62678	-.55468
15	-.38268	-.38268	-.28982	-.42473	-.42473	-.33635	-.46109	-.38207
16	-.19509	-.19509	-.09786	-.23797	-.23797	-.14649	-.27324	-.19478

Table 8. Converged numerical solutions and zone-averaged asymptotic solutions for the experiments of Table 7.

makes it possible to compute $F_{EO}(u_L,u_R)$ explicitly, while $F_G(u_L,u_R)$ must be determined iteratively.

The Engquist-Osher scheme, on the other hand, requires two interior points in a discrete stationary shock [5], while Godunov's scheme probably requires only one (this has not yet been proven).

For the Euler equations, however, Roe's more drastic simplification of Godunov's method will pay off, even though the scheme must be somewhat modified in order to reject (almost) stationary expansion shocks. Spreading the expansion waves in the approximate Riemann solution underlying the scheme will have the desired effect.

The first-order schemes, when formulated as in Section 6, have the potential of achieving any desired order of spatial accuracy in a steady numerical solution. To what degree this potential can be realized for the Euler equations is at present not clear. Meanwhile, the second-order two-step schemes, intended primarily for solving transient problems, outperform the first-order schemes in obtaining a steady solution for Burgers' equation. Some experiments for the Euler equations with both kinds of schemes are reported in [13].

All schemes discussed in this paper are explicit. When using their numerical flux-functions in an implicit configuration, which may be desirable in approaching a steady state, the above recommendations do not automatically carry over. As noted by Engquist and Osher [4], the non-smooth dependence of $F_G(u_L,u_R)$ on its arguments in the case (iii) of a transonic shock, that is $F_G(u_L,u_R) \in C^{(0)}$, complicates the inversion of the implicit difference equations. In contrast, $F_{EO}(u_L,u_R) \in C^{(1)}$ in all cases (i), (ii) and (iii).

Acknowledgment

The ideas of Steve Hancock (Physics International, San Leandro, CA) and Dick van Albada, NRAO, Charlottesville, VA), embodied in eqs. (40) and (42), respectively, are greatly appreciated, while discussions with Stanley Osher (UCLA) strengthened my belief in the treatment of source terms discussed in Section 6.

References

1. S. K. GODUNOV, Mat. Sb. 47 (1959), 271; also: Cornell Aeronautical Lab. (Calspan) Translation.

2. S. K. GODUNOV, A. W. ZABRADYN and G. P. PROKOPOV, Zhur. Vycisl. Mat. Fiz. 1 (1961), 1020; also: Cornell Aeronautical Lab.(Calspan) Translation.

3. A. HARTEN, P. D. LAX and B. VAN LEER, "Upstream differencing and Godunov-type schemes for hyperbolic conservation laws," ICASE Report in preparation.

4. B. ENGQUIST and S. OSHER, Math. Comp. 34 (1980), 45-75.

5. S. OSHER and F. SOLOMON, "Upwind difference schemes for hyperbolic systems of conservation laws," UCLA preprint, submitted to Math. Comp., 1980.

6. P. L. ROE, "The use of the Riemann problem in finite-difference schemes," Proceedings of the Seventh International Conference on Numerical Methods in Fluid Dynamics, Springer-Verlag, to appear (1981).

7. P. L. ROE, "Approximate Riemann solvers, parameter vectors and difference schemes," to appear in J. Computational Phys. (1981).

8. E. M. MURMAN, AIAA J., 12 (1974), 626-633.

9. S. L. HANCOCK, private communication, 1980.

10. B. VAN LEER, J. Computational Phys., 32 (1979), 101.

11. B. VAN LEER, J. Computational Phys., 23 (1979), 276.

12. G. D. VAN ALBADA, private communication, 1981.

13. G. D. VAN ALBADA, M. Y. HUSSAINI, W. W. ROBERTS, B. VAN LEER, and T. ZANG, "Finite-difference solution of a galactic flow problem," ICASE Report, in progress (1981).

E R R A T U M

page 28, line 5 from bottom: first-order read second-order
page 28, line 3 from bottom: second-order read first-order

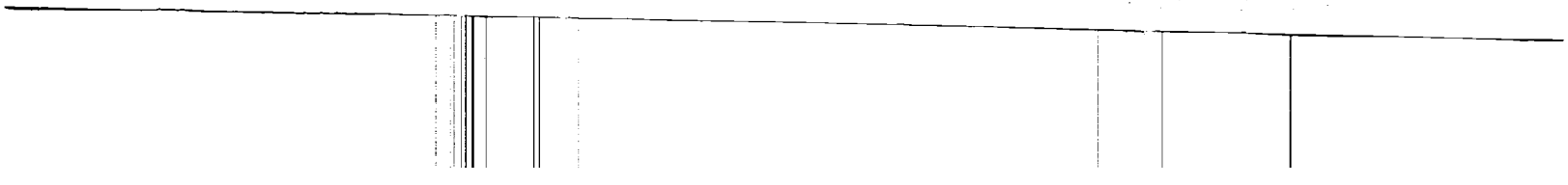

End of Document